Biosensors and Bioelectronics 261 (2024) 116505

Contents lists available at ScienceDirect

Biosensors and Bioelectronics

journal homepage: www.elsevier.com/locate/bios

Microsphere lens array embedded microfluidic chip for SERS detection with simultaneous enhancement of sensitivity and stability

Zhenyong Dong [a,b,1], Xiaoxian Liu [a,b,d,1], Song Zhou [e], Yifan Zhu [a,b], Jin Chen [d], Yukai Liu [a,b], Xiao Ren [a,b], Yan-qing Lu [a,*], Rui Xiao [d,**], Guanghui Wang [a,b,c,***]

[a] College of Engineering and Applied Sciences, Nanjing University, Nanjing, 210093, PR China
[b] Key Laboratory of Intelligent Optical Sensing and Integration of the Ministry of Education, Nanjing University, Nanjing, 210009, PR China
[c] Nanjing Drum Tower Hospital, The Affiliated Hospital of Nanjing University Medical School, Nanjing, 210008, PR China
[d] State Key Laboratory of Pathogen and Biosecurity, Beijing Institute of Microbiology and Epidemiology, Beijing, 100071, PR China
[e] Jiangsu Key Laboratory of Advanced Manufacturing Technology, Faculty of Mechanical and Material Engineering, Huaiyin Institute of Technology, Huai'an, 223003, PR China

ARTICLE INFO

Keywords:
Surface enhanced Raman spectroscopy
Barium titanate microspheres array
SERS microfluidic chip
Multiple focus arrays
Photonic nano-jets

ABSTRACT

Surface enhanced Raman spectroscopy (SERS) utilizes the fingerprint features of molecular vibrations to identify and detect substances. However, in traditional single focus excitation scenarios, its signal collection efficiency of the objective is restricted. Furthermore, the uneven distribution of samples on the SERS substrate would result in poor signal stability, while the excitation power is limited to avoid sample damage. SERS detection system always requires precise adjustment of focal length and spot size, making it difficult for point-of-care testing applications. Here, we proposed a SERS microfluidic chip with barium titanate microspheres array (BTMA) embedded using vacuum self-assembled hot-pressing method for SERS detection with simultaneous enhancement of sensitivity and stability. Due to photonic nano-jets and directional antenna effects, high index microspheres are perfect micro-lens for effective light focusing and signal collecting. The BTMA can not only disperse excitation beam into an array of focal points covering the target uniformly with very low signal fluctuation, but enlarge the power threshold for higher signal intensity. We conducted a proof-of-principle experiment on chip for the detection of bacteria with immuno-magnetic tags and immuno-SERS tags. Together with magnetic and ultrasonic operations, the target bacteria in the flow were evenly congregated on the focal plane of BTMA. It demonstrated a limit of detection of 5 cells/mL, excellent signal reproducibility (error~4.84%), and excellent position tolerance of 500 μm in X–Y plane (error~5.375%). It can be seen that BTMA-SERS microfluidic chip can effectively solve the contradiction between sensitivity and stability in SERS detection.

1. Introduction

Surface Enhanced Raman spectroscopy (SERS) based on electromagnetic enhancement and chemical enhancement can enhance the molecular vibration signal by 10^6-10^{14} times, and use the fingerprint property of molecular vibration to identify the target substances, with the advantages of non-contact, high sensitivity, high selectivity and single molecule detection (Kim et al., 2022; Liu et al., 2022; Mungroo et al., 2015; Xie et al., 2024; Yu et al., 2024). In practice, SERS commonly utilize a functionalized substrate and a focused beam featuring a small spot size of few microns and a limited numerical aperture (NA) for sample detection (Langer et al., 2020). There are some limitations for its applications:1), The substrate is costly and always only for one-time use; 2), Due to the uneven distribution of samples within the SERS substrate especially for very low-density case, there is a non-negligible possibility that no sample appears in the focus region, which may result in significant signal fluctuations in the detection, leading to the decreasing of system stability. On the other side, increasing the

* Corresponding author.
** Corresponding author.
*** Corresponding author. College of Engineering and Applied Sciences, Nanjing University, Nanjing, 210093, PR China.
E-mail addresses: yqlu@nju.edu.cn (Y.-q. Lu), ruixiao203@163.com (R. Xiao), wangguanghui@nju.edu.cn (G. Wang).
[1] These authors contributed equally to this paper.

https://doi.org/10.1016/j.bios.2024.116505
Received 8 February 2024; Received in revised form 25 May 2024; Accepted 15 June 2024
Available online 15 June 2024

coverage area of the spots may enhances stability, but at the cost of the signal intensity. There is a tradeoff between stability and amplification; 3), Moreover, for single-focus detection system, the highly concentrated laser power also would lead to sample damage, thereby total signal intensity is always limited by the local power density threshold; 4), The SERS detection process is always very complicated. The operators need to manual focusing and search for samples with highest intensity, which in some distance is a subjective criterion; 5), There is no on-chip integration of the whole SERS detection process for point-of-care applications. Hence, a portable SERS system, which is facile to achieve on-chip integration and has compatibility with stability and signal gain, is urgently desired (Fan et al., 2020).

Dielectric microspheres (DMs) are perfect micro-lens for excellent localized light amplification, which can provide good Raman enhancement capabilities without plasma assistance, due to the contributions of photonic nano-jets (PNJs), optical whispering-gallery modes and directional antenna effects (DAEs) (Pahl et al., 2022; Wang et al., 2022). Based on PNJs effect, DMs with relatively large index difference can generate a highly focused beam at very small distance with large numerical aperture (NA), converging the incident light into tens nanometers, increasing the optical power density substantially onto the neighboring target objects, exciting and collecting the Raman signals most effectively (Du et al., 2011; Gašparić et al., 2019; Geints et al., 2018; Mi et al., 2022; Ruzankina et al., 2022; Yang et al., 2016; Yousefi et al., 2021; Zhang et al. 2020, 2022). Further due to DAEs effect, DMs can restrict the scattered light to a narrow region with a small divergence angle, thus maintaining the signal-to-noise ratio, reducing the offset of the focal plane position relative to the sample surface, and achieving better signal amplification and stability in the vertical direction (Yan et al., 2015). Moreover, a dielectric microspheres array (DMA) can uniformly disperse the single focused spot into an array of focal points evenly covering the target with very low signal fluctuation and high stability. This distributed multi-focus configuration could enlarge the power threshold for higher signal intensity and better sensitivity. If the DMA can be productively fabricated and easily integrated with detection system, it will be an ideal portable SERS system with better practicality and feasibility.

SERS Microfluidic chips (SERS-LoC) can simplify the manual operations which could greatly improve the level of system integration (Ahi et al., 2022; Huang et al., 2015; Ma et al., 2021; Panneerselvam et al., 2022; Wang et al., 2020; Wu et al., 2024; Xiong et al., 2018; Yang et al., 2022). The whole process including sample enrichment, sample washing, and SERS detection process could be integrated on chip, solving the problems of poor signal reproduction in sample analysis and easy sample contamination in open system, and achieving rapid and sensitive detection of microliter or even nanoliter of sample liquid. On the other side, the high refractive index DMA can be embedded in the lower index microfluidic channels for effective detection system integration, which has the unique advantages in solving the problems faced by SERS.

In this paper, we have designed and fabricated a BTMA-SERS microfluidic chip with high index barium titanate microsphere arrays (BTMA) embedded in the top layer of polymethylmethacrylate (PMMA) plate channel, using the vacuum self-assembly hot-pressing method. BTMA can evenly disperse a single focused spot into multiple focus arrays with uniformly Raman signal excitation and wider signal collection angle. By applying the magnetic and ultrasonic operations within the chip, the target samples homogeneously concentrated at the bottom of the channel also on the focal plane of BTMA microlens, achieving the double improvement of signal sensitivity and stability. Finally, we conducted a proof-of-principle experiment on chip with sample capture by using Fe_3O_4@Au magnetic nanoparticles (MNPs), and ultrahigh sensitive detection of *Pseudomonas aeruginosa* (*PA*) bacteria by using SERS probe. After the whole process, *PA* was detected with a limit of detection (LOD) of 5 cells/mL, with 4 times signal enhancement, very small relative standard deviation (RSD) of signal reproducibility of 4.84%, and excellent position tolerance of 500 μm in X–Y plane (RSD~5.375%). Receiver operating characteristic (ROC) curve with an area under the curve (AUC) of 1 indicated the high specificity and accuracy of the chip for determining PA clinical samples. It can be seen that our BTMA-SERS microfluidic chip can effectively solve the contradiction between sensitivity and stability in SERS detection, and has the potential for clinical application.

2. Materials and methods

2.1. Materials

Barium titanate ($BaTiO_3$) microspheres with a diameter of 180–200 μm were supplied by Cospheric LLC (California, USA). Ethanol anhydrous (C_2H_6O), phosphate buffer saline (PBS) and Tween 20 were purchased from Shanghai Macklin Biochemical Technology Co., Ltd (China). Octadecyltrimethoxysilane ($C_{21}H_{46}O_3Si$) and acetone (CH_3COCH_3) were purchased from TCI Shanghai. Chloroauric acid tetrahydrate ($HAuCl_4{\cdot}4H_2O$), trisodium citrate (TSC), and hydroxylamine hydrochloride ($NH_2OH{\cdot}HCl$) were purchased from Shanghai Sinopharm Chemical Reagent Co., Ltd (China). Polyethyleneimine branched (PEI, MW 25 kDa), bovine serum albumin (BSA), polyvinylpyrrolidone (PVP, MW 40 kDa), N-(3-dimethylaminopropyl)-N′-ethylcarbodiimide hydrochloride (EDC), N-hydroxysuccinimide (NHS), 2-(N-morpholino) ethanesulfonic (MES), and DTNB were obtained from Sigma-Aldrich (USA). Monoclonal anti-pseudomonas aeruginosa antibodies (Catalog #JNDX, 12007) were bought from Jiangnan university (China). Sputum digestion solution (R30485) were purchased from Shanghai yuanye Bio-Technology Co., Ltd. The blood samples of healthy male mice (BLAB/c) were provided by Beijing. The sputum clinical samples were provided by Nanjing Drum Tower Hospital.

2.2. Preparation of immuno-Mag@Au NPs

We modified the PEI-mediated seed growth method to prepare MNPs with good dispersion and high stability (Liu et al. 2020, 2023). In the preparation method shown in Fig. S1, the cationic polymer PEI was first coated on the Fe_3O_4 surface to form a positively charged interlayer. Then, negatively charged 13 nm colloidal gold (AuNPs) are densely fixed on the Fe_3O_4 surface to form seeded magnetic particles by electrostatic forces combined with the positively charged PEI. Finally, a rough and continuous layer of gold shell outside the magnetic core is obtained by reductive deposition of Au^{3+} on the seeded surface. Subsequently, 50 μM MUA bind to the surface of MNPs with Au–S bond under optimal ultrasonic use, providing a large number of sites for antibody coupling.

2.3. Preparation of immuno-SERS tags

In this work, we prepared immuno-Au SERS tags using 40 nm AuNPs was used to prepared immuno-Au SERS tags as molecular recognition and quantitative detection tool according to the synthetic steps shown in Fig. S2. AuNPs (40 nm) were fabricated through the citrate reduction method. Briefly, 1 mL of trisodium citrate (1%, w/v) was added rapidly to the 100 mL of boiling solution of HAuCl4 (0.01 wt%) with stirring. The suspension was boiled for 15 min and then allowed to reach thermal equilibrium at room temperature. 20 μM of DTNB was added and vigorously stirred for 4 h to obtained Au-DTNB NPs. Then, 2 mL prepared Au-DTNB solution was resuspended in MES solution (2 mM, pH 5.4) containing 10 mM EDC and NHS to activate carboxyl groups for 15 min. The products collected by centrifugation (4600 rpm, 7 min) were suspended in PB (2 mM, pH 7) buffer to coupling with 10 μg of the capture antibody under shaking for 2 h. Excessed carboxyl sites were blocked by 50 μL of 10% BSA. The immuno-AuNPs were collected by centrifugation (4700 rpm, 6 min) and resuspended with 200 μL of PB buffer.

2.4. Preparation of BTMA by vacuum self-assembly hot-pressing method

This process utilized the vacuum self-assembly hot-pressing method to prepare BTMA, involving the creation of a 2 mm diameter hollow circle mold fixed on a slide. Anhydrous ethanol is applied to this area, and barium titanate microspheres (BTM) are evenly spread over the ethanol-dripped surface. Due to liquid surface tension, BTM self gravity and total lateral forces (capillary force, electrostatic repulsion and spatial potential resistance), BTM gradually covers the circular area. A PMMA plate is placed over the mold, and the assembly is sealed in a vacuum bag for evacuation. This vacuum treatment eliminates air bubbles between BTMs, enhancing their compactness and stability. The sealed BTMA mold is heated with 160 °C for 1.5 h on a thermostatic table with pressure applied, and after cooling naturally in the air, the more compact and stable BTMA was produced.

2.5. Theoretical simulation

COMOSL Multiphysics field finite element method was used to theoretically simulate the light scattering path of BTMA. The 785 nm wavelength is used as the excitation light source in the model, which is incident on the microspheres from top to bottom from PMMA. With perfectly matched layer and periodic boundary conditions, the excitation light incident on the microspheres generates Mie scattering and forms a photonic nano-jet. In the study of DAEs, an electric dipole with a wavelength of 877 nm was placed on the surface of a silicon wafer as a point source emission point to simulate the modulation of scattered light by microspheres.

3. Results and discussion

3.1. Working Mechanism of BTMA-SERS microfluidic chip

The fundamental mechanism and detection technique of the BTMA-SERS microfluidic chip proposed is illustrated in Fig. 1. Firstly, when the BTMA are covered by a large-diameter laser beam, the BTM acts as a micro-lens to generate the PNJs effect, converging the incident light and producing highly focused multiple focus arrays. Compared with the traditional single focusing point scenario, the multiple-focus arrays generated by BTMA, on the one hand, can completely cover the samples on the SERS substrate, avoiding the instability of the detection signal caused by the uneven distribution of the samples; on the other hand, it scatters the power density of the single focusing beam, amplifying the power threshold of the Raman detection process, consequently preventing damage of the samples owing to the focused beam. For large diameter BTMA with large refractive index, which produce a directional antenna effect that can limit the scattered light closer to parallel propagating waves. Meanwhile, BTMA has a larger NA than standard lens probes, contributing to a significant increase in light collection efficiency (Fig. 1a and b). More importantly, BTMA with localized PNJs and DAEs can effectively enhance Raman scattering. The excitation light generates PNJs at the bottom of the BTMA, which significantly enhances the excitation intensity. Under the effect of PNJs, MNPs-*PA*-Au@DTNB aggregated at the bottom of the BTM arrays generates a high-intensity localized surface plasmon resonance. Thus, we used BTMA to detection sample, achieving a four times enhanced Raman signal (Fig. S3). DAEs restrict the scattered light to a narrow region with a small divergence angle (±4.5°), effectively increasing the Raman scattering intensity in the optical axis direction and enabling efficient far-field energy collection. Meanwhile, the offset of the focal plane position relative to the sample surface is reduced and Raman detection in the vertical position without precise focusing is permitted. Then, the PEI-mediated seed growth method was improved in this study, and well-dispersed MNPs were prepared for rapid capture and enriched *PA*. Antibody-conjugated Au NPs (40 nm) SERS tags were acted as recognition module to form a sandwich structure with the *PA* captured by the MNPs. And the measurable SERS signal at 1336 cm^{-1} generated by the encoded Raman reporter molecule (DTNB) was used for quantitative analysis. (Fig. 1c).

Finally, we utilized vacuum self-assembly hot pressing to embed the microsphere arrays in polymethyl methacrylate (PMMA) and encapsulated them with the runner layer and other components to form the

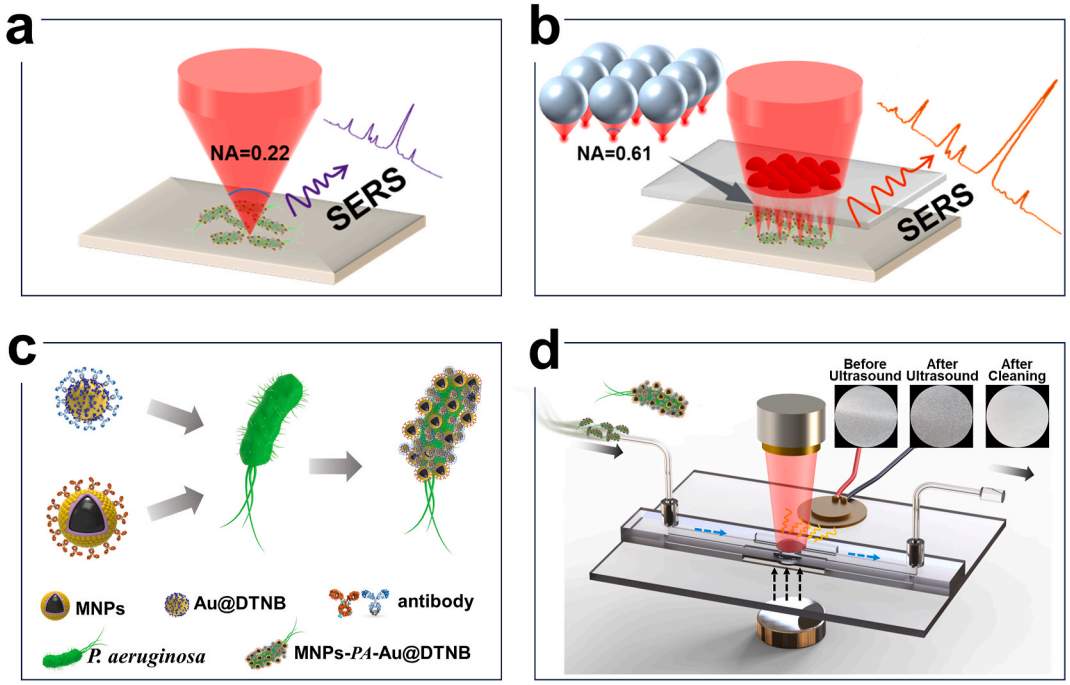

Fig. 1. Working Mechanism of BTMA-SERS microfluidic chip. (a) Traditional single focus covering samples on SERS substrates. (b) Large NA BTMA form multiple focus arrays evenly covering samples on SERS substrates. (c) Mechanism of formation of MNPs-*PA*-Au@DTNB sandwich structure. (d) The overall conceptual diagram of BTMA-SERS microfluidic chip and its detection mechanism.

BTMA-SERS microfluidic chip (Fig. 1d). In the influence of the magnetic field, the MNPs-*PA*-Au@DTNB was formed uneven aggregation within the chip detection area. To optimize this phenomenon, ultrasound vibration was introduced to promote more homogeneous aggregation of the MNPs-PA-Au@DTNB, and to assist in the cleaning of the MNPs-*PA*-Au@DTNB after the detection was completed, facilitating the reuse of the chip (Fig. S4 and Video SI). The SERS intensity at 1336 cm^{-1} for different concentrations of *PA* was measured by a portable Raman spectrometer and the reproducibility of the Raman signal was measured and analyzed. Besides, the SERS signal intensity at 1336 cm^{-1} was tested to maintain a good stability when the laser beam produced a lateral movement (±500 μm), using 10^5 cells/mL concentration of *PA* as a sample.

Supplementary video related to this article can be found at https://doi.org/10.1016/j.bios.2024.116505

3.2. Characterization of immuno-Mag@Au NPs

High-resolution transmission electron microscope (HRTEM) and energy dispersive spectrometer (EDS) elemental mapping analysis were

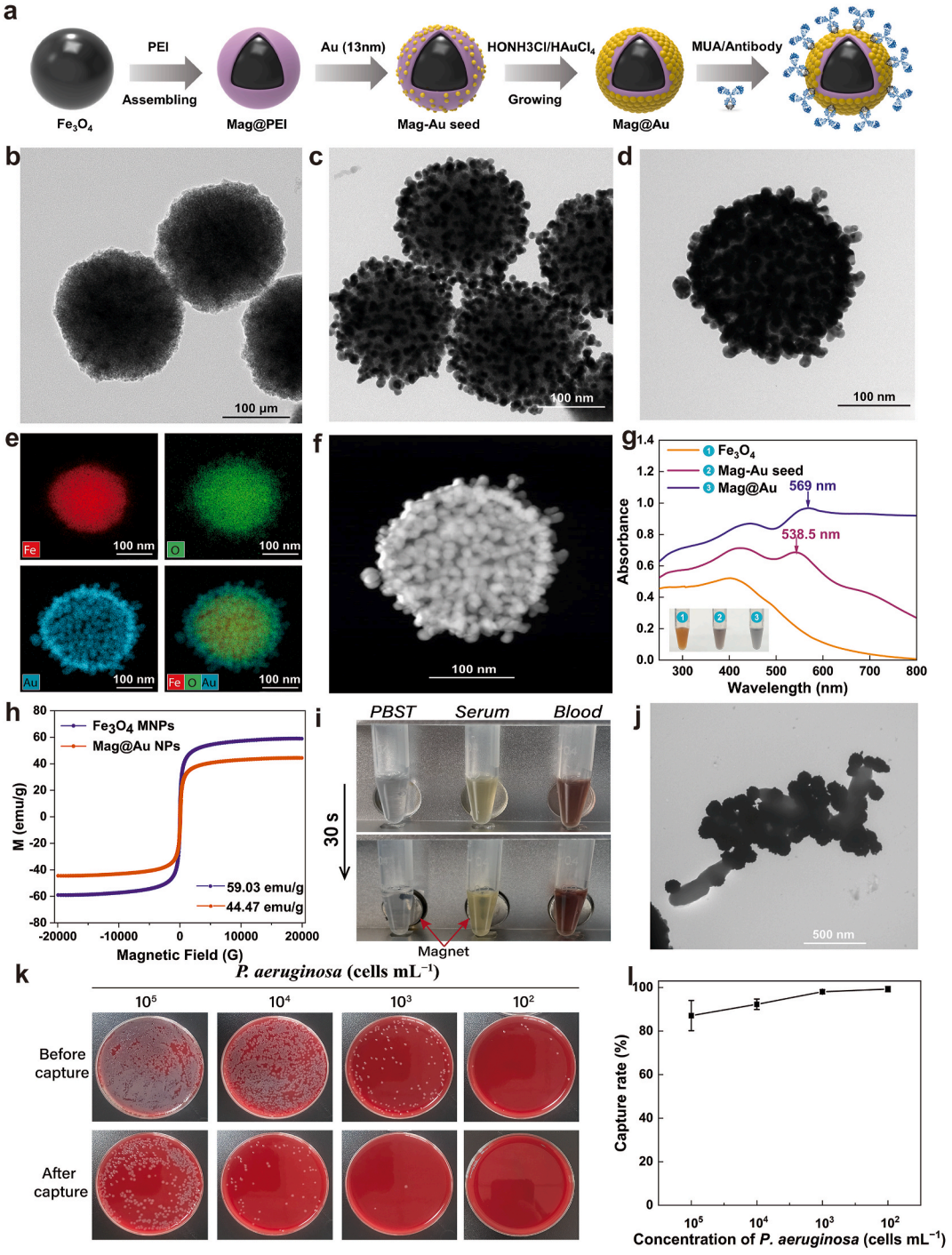

Fig. 2. Characterization of MNPs. (a)–(c) HRTEM images of Fe_3O_4 MNPs, Mag-13 nm Au seeds and MNPs. (d) Elemental mapping images of MNPs. (e) HADDF image of a single MNP. (f) UV–vis spectra of Fe_3O_4, Mag-13 nm Au seeds and MNPs. (g) Magnetic hysteresis curves of Fe_3O_4 and MNPs. (h) Magnetic properties of MNPs in complex samples. (i) TEM image results of *PA* captured by MNPs. (j)–(k) Results of capture efficiency of immuno- MNPs s at *PA* concentrations of 10^2 cells/mL-10^5 cells/mL. The error bars indicated the standard deviations calculated from three independent experiments.

used to characterize the prepared MNPs. Fig. 2a shows the HRTEM image of the Fe_3O_4 magnetic particles (Fe_3O_4 MNPs), which clearly shows that the diameter of the Fe_3O_4 MNPs is about 190 nm. Fig. 2b shows the HRTEM image of the seeded Fe_3O_4 MNPs, which shows that the 13 nm NPs are densely adhered to the surface of the Fe_3O_4 after PEI coating. The dense gold seeds provided sufficient sites for the subsequent anisotropic growth of the gold nano-shells. Fig. 2c shows a HRTEM image of the obtained MNPs with a distinct core-shell nanostructure and rough surface. The EDS spectrum (Fig. S5) indicates that the components of MNPs are only Fe, O and Au used. Elemental mapping image in Fig. 2d further demonstrated that Au (blue) was densely and uniformly distributed in the external surface the Fe (red) and O (green) cores. Furthermore, high-angle annular dark-field scanning TEM (HAADF) image shown in Fig. 2e confirms that the MNPs core surface is coated with an Au shell.

The dynamic synthesis of Au shell with continuous protuberances was further confirmed by UV–vis spectroscopy. As shown in Fig. 2f, the initial SPR absorption peak of Mag-Au seeds was located at 538.5 nm, and after the formation of the rough Au shell layer, the absorption peak was significantly red-shifted to 569 nm, which was attributed to the adoption of the magnetic core-shell hybrid nanoparticle structure with nanogaps, and the SERS activity of MNPs was significantly improved. Meanwhile, we also used zeta potential results for the monitoring of the corresponding preparation steps of MNPs (Fig. S6). Fig. 2g depicted that the magnetic saturation (MS) value of MNPs was 44.47 emu/g, which is only 24.7% lower than that of Fe_3O_4 MNPs (59.03 emu/g), maintaining a high magnet content. No hysteresis lines appeared in the graphs, indicating that the superparamagnetism and strong magnetic responsiveness of MNPs endowed it with the ability to rapidly and completely separate analyte from complex solutions. As shown in Fig. 2h, MNPs can be completely separated from each of the three composite samples (PBST buffer, serum, and whole blood) within 30s under the action of an applied magnetic field. We compared the Raman signals when different concentrations of MNPs were used for detection *PA* and obtained the optimal concentration of 15 μM for MNPs (Fig. S7). The capture of *PA* by 15 μL MNPs is shown in Fig. 2i–k. The average capture efficiency of MNPs exceeds 90% at *PA* concentration between 10^2 and 10^5 cells/mL, especially with the highest recorded of 99% at 10^2 cells/mL. Manual spreading of plates inevitably has errors, resulting in a high experimental error in the capture efficiency of high concentrations of *PA*. In conclusion, monodisperse MNPs have been successfully synthesized and a volume of 15 μL demonstrates high bacterial capture efficiency within 15 min, making it suitable for pathogenic microorganism detection.

3.3. Characterization of immuno-SERS tags

Immuno-SERS tags typically consist of a metal nanosubstrate, an organic Raman reporter molecule and a bio-recognition element (Bai et al., 2020; Spaziani et al., 2023; Xie et al., 2023). The significant SERS enhancement attributed to the electromagnetic mechanism occurring between Raman reporter molecule and noble metal (Song et al., 2018; Wang et al., 2015). The dynamic light scattering (DLS) result shown in Fig. 3a confirmed the average diameter of synthesis AuNPs. DTNB with large Raman scattering cross section and the absence of fluorescence interference was the first choice for the Raman reporter molecule. The SERS enhancement factor (EF) of Au at 1336 cm^{-1} from DTNB was calculated to be 1.15×10^5 by using a previously reported method, which could meet the requirement of sensitive detection (Supporting information S1 and Fig. 3b). After DTNB was encoded on AuNPs by the Au–S bond, the *PA* antibody was directly combined with the carboxyl groups of Au-DTNB NPs through EDC/NHS chemistry. Zeta potential results (Fig. S8) successfully monitored the formation of the immuno-Au SERS tags. Moreover, we evaluated the SERS intensity and stability of immuno-Au SERS tags at 5μM–500μM of DTNB coding concentrations. As illustrated in Fig. 3c, the Raman signal was no longer significantly enhanced or even decreased when DTNB concentration exceeded 40 μM. Notably, the Au colloid changed color at this time, indicating the agglomeration precipitation of particles. Hence, 40 μM of DTNB was the optimal encoded concentration.

3.4. Fabrication and Characterization of BTMA-SERS microfluidic chip

We have fabricated a barium titanate microsphere arrays SERS microfluidic chip for fast, stable and ultrahigh resolution bioanalysis (Fig. S9). The BTMA are embedded into PMMA by vacuum self-assembly hot-pressing method (Fig. 4a and Fig. S10). The vacuum treatment can reduce the air bubbles between the BTMs, which makes the BTMA arrangement more compact and reduces the light loss (Fig. S11). The indentation depth and focal length of the BTMs varied with the hot-pressing time. And when the hot-pressing time is 1.5 h, the microsphere indentation depth is about 100 μm, the prepared BTMA were neatly arranged, compact and stable, and not easy to fall off (Fig. 4b–c and Fig. S12). The location of the BTMA in the chip is shown in Fig. 4d. It is worth noting that the chip utilizes strong magnetic and piezoelectric ceramic vibrator (PCV) have been employed to assist in the controlled homogeneous aggregation of the MNPs-*PA*-Au@DTNB sandwich structure (Fig. S13) and are located underneath and on the surface of the bottom silicon slice, respectively. Furthermore, the ultrasonic vibration of the PCV can aid in cleansing the sandwich structure of MNPs-*PA*-Au@DTNB, thereby facilitating the chip's reusability (Fig. S14 and Video SI).

For further the light scattering mechanism of BTMA in the chip, the PNJs and DAEs of BTMA for enhanced Raman scattering are theoretically simulated by COMSOL Multiphysics field finite element method. The modeling principle is shown in Fig. 4e, where the excitation light source is incident on the microsphere surface from top to bottom by

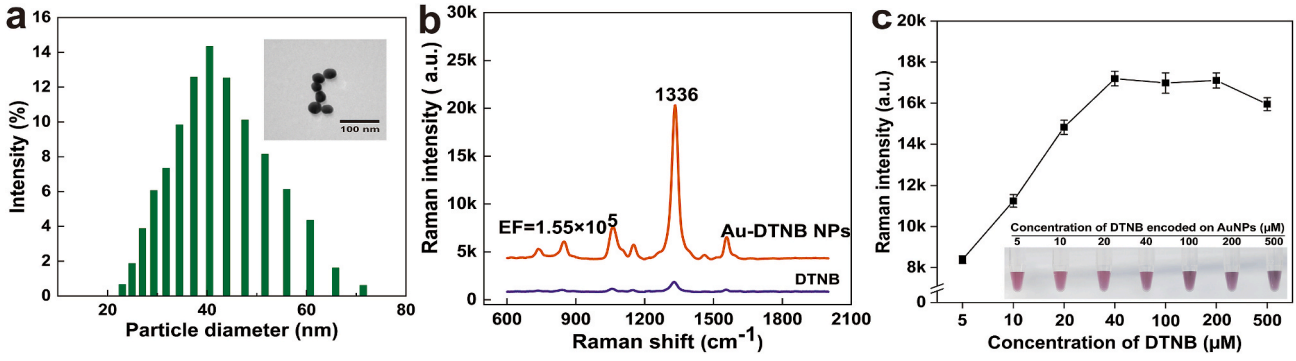

Fig. 3. Characterization of immuno-SERS tags. (a) DLS distributions of Au NPs. (b) Raman spectra of DTNB molecules on different substrates: 0.1 M DTNB on Si substrate (purple line), and 10^{-5} M DTNB on Au (Orange line). (c) Raman signal and color changes of immuno-Au SERS tags at different concentration of DTNB. The error bars indicated the standard deviations calculated from three independent experiments.

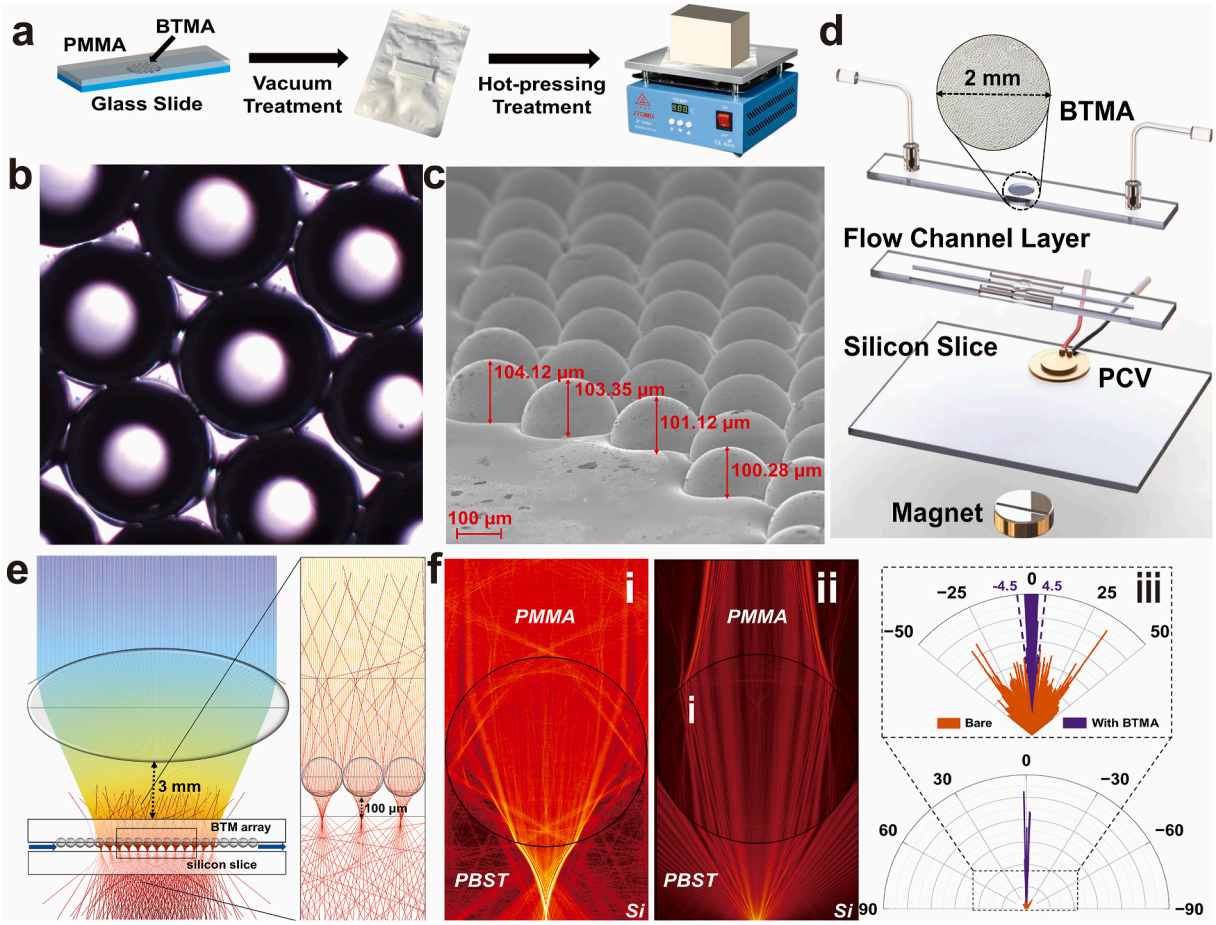

Fig. 4. Fabrication and Characterization of BTMA-SERS microfluidic chip. (a) The process of the vacuum self-assembly hot-pressing method. (b) The microscopic view of BTMA embedded in PMMA layer. (c) The Scanning electron microscope images of BTMA which shows the Embedding depth of microspheres. (d) The structure of each part of BTMA-SERS microfluidic chip, which the 2 mm BTMA is embedded in the top cover of the flow channel. (e) The modeling of BTMA for the light focusing effect. (f) The light scattering mechanism of BTMA in the device: (i) Photonic nano-jets of BTMA; (ii) Directional antenna effects of BTMA; (iii) The BTMA limits the Raman scattering emission angle to ±4.5°.

PMMA and the bare BTMA is in contact with the fluid. With the focusing property of the microsphere lens, when the excitation light is incident on the microsphere, a PNJ is generated at the bottom of the BTMA (the focal length is about 100 μm), which significantly enhances the excitation intensity (Fig. 4f). In addition, the microsphere is an optical directional antenna that limits the Raman scattering emission angle to ±4.5°, which effectively improves the Raman scattering intensity in the direction of the optical axis and interns efficient far-field energy collection (Fig. 4f).

3.5. *PA* detection capability of BTMA-SERS microfluidic chip

P. aeruginosa is an immunocompromised opportunistic pathogen responsible for 10 percent of hospital-acquired infections and is found mainly in body fluids such as sputum and wound secretions (Li et al., 2022). Early accurate and highly sensitive detection is essential. Hence, we select *PA* as the target to verify the detection performance of BTMA-SERS microfluidic chip in this work. The specific operation process is illustrated in Fig. 5a. After *PA* was completely captured within the incubation time of 15 min, immuno-Au SERS tags were added to the Mag@Au-*PA* complex to form a MNPs-*PA*-Au@DTNB sandwich structure. The incubation time and addition amount of immuno-Au tags was optimized to obtain the highest binding efficiency and improve SERS detection performance. As displayed in Fig. S15, the highest Raman signal and SNR can be achieved with a reaction time of 20 min, which was finally selected as the duration of SERS tags binding. Fig. S16 shown the Raman spectrum corresponding to addition amounts of SERS tags. At 10^5 cells/mL of *PA*, the Raman signal was enhanced and linearly correlated with the increase of SERS tags range from 10 μL to 100 μL. Significantly, the Raman signal tends to be saturated when the tags were above 90 μL. Considering the realization of higher concentration of *PA* detection, the volume of SERS tags used in this experiment was optimized 100 μL.

Next, we built the experimental platform shown in Fig. S17 and used the experimental method of supporting information SI2 to measure the various performances of the BTMA-SERS microfluidic chip. It is worth noting that we have hydrophobic treatment on the chip to avoid liquid remaining, while using alcohol, deionized water and nitrogen gas to rinse the chip sequentially to eliminate the aggregation of tiny impurity particles. In this process, we also have assisted the cleaning by means of ultrasonic vibrations generated from an ultrasonic device fitted on the chip. Finally, undesired aggregation is avoided to ensure the accuracy and stability of the experiment. Fig. 5b was the average Raman spectra measured from BTMA-SERS microfluidic chip, showing that the SERS intensity gradually increased with increasing bacteria concentration (5–10^7 cells/mL). Based on the results, we plotted the calibration curve between the SERS intensity of DTNB at 1336 cm^{-1} and the logarithm of the *PA* concentration (0-10^7cells/mL) at Fig. 5c. The BTMA-SERS microfluidic chip possess a good linear relationship range from 5 to 10^7cells/mL with a linear correlation coefficient (R^2) of 0.995. According to the calculated blank control signal and triple standard deviation (IUPAC protocol), The LOD and limit of quantification (LOQ) of BTMA-SERS microfluidic chip are 5 cells/mL and 6 cells/mL,

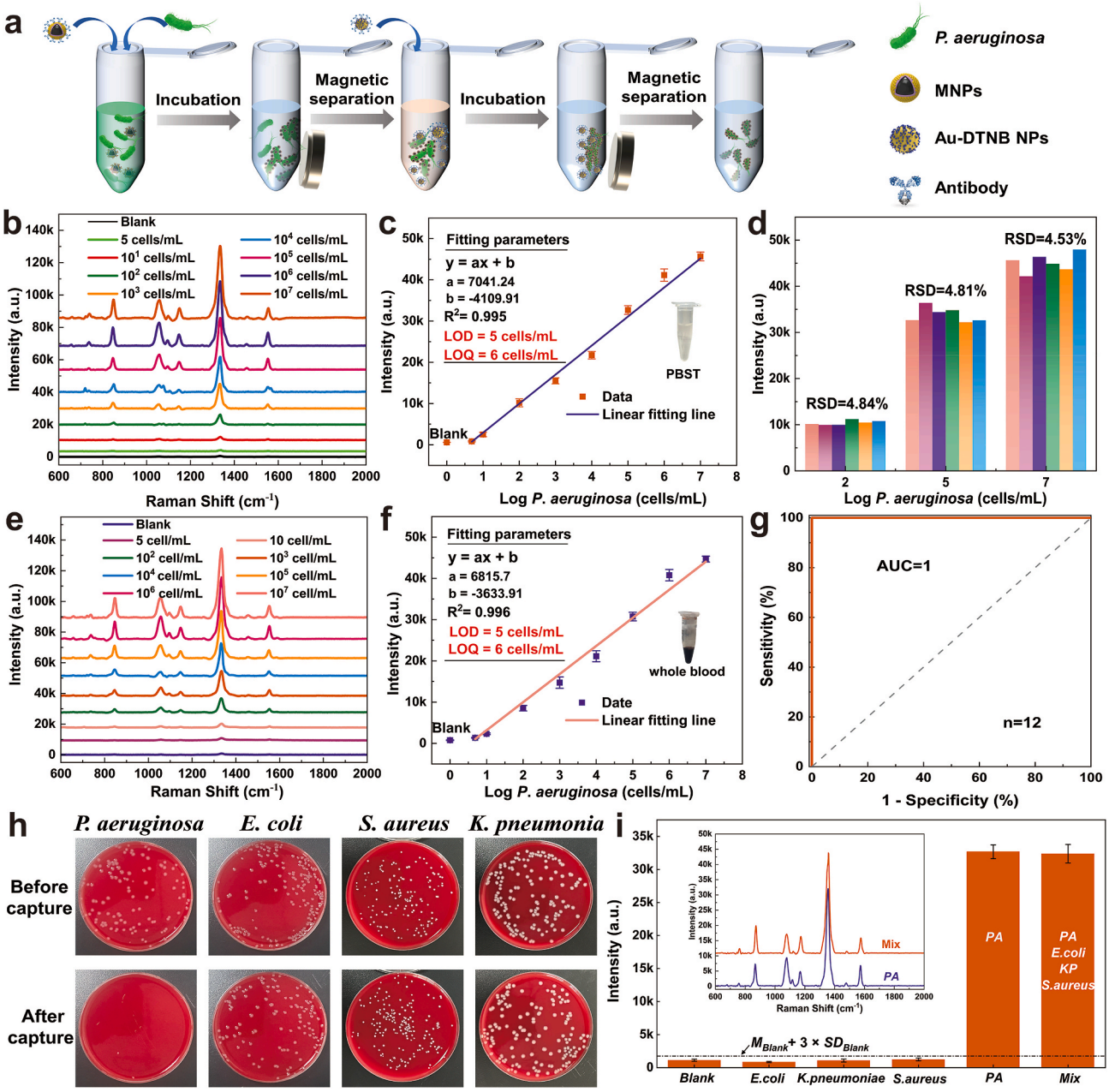

Fig. 5. BTMA-SERS microfluidic chip shows ultra-high resolution and specificity in *PA* detecting. (a) Incubation process for MNPs-*PA*-Au@DTNB. (b) Average SERS spectra of *PA* detected using BTMA-SERS microfluidic chip. (c) Corresponding calibration curve for different concentration of *PA*. (d) Reproducibility of the BTMA-SERS microfluidic chip for different concentrations of *PA* (10^2cells/mL, 10^5cells/mL, 10^7cells/mL). (e) Average SERS spectra of *PA* detected using BTMA-SERS microfluidic chip in whole blood of healthy mice. (f) Corresponding calibration line for different concentration of *PA*. (g) ROC curve. (h) Plate counting results of four bacteria before and after immuno-Mag@Au capture. (i) The results of the specificity test for the four bacteria. The error bars indicated the standard deviations calculated from three independent experiments.

respectively, with strong test stability. Six experimental groups containing three concentrations of *PA* (10^2cells/mL, 10^5cells/mL, 10^7cells/mL) were repeated to assess the reproducibility of different batches of the proposed BTMA-SERS microfluidic chip. As demonstrated in Fig. 5d, the relative standard deviations (RSD) value of SERS intensity was 4.84%, 4.81%, and 4.53%, respectively, indicating the superior reproducibility of BTMA-SERS microfluidic chip and the ability to accurate quantitative detection.

As a potential clinical pathogen detection tool, the analytical performance of BTMA-SERS microfluidic chip in real blood samples needs to be validated. Due to the strategy of first capturing *PA* with immuno-MNPs in this work, subsequent SERS detection is not affected by complex components. Samples of bacteria at different concentrations (10^7 to 0 cells/mL) in serial dilution were spiked to the whole blood of healthy mice and then tested in the proposed system. As shown in Fig. 5e and f, the SERS intensity and dynamic change trend were similar to the results in buffer solution, which proved that the LOD and LOQ of BTMA-SERS microfluidic chip in whole blood detection were 5 cells/mL and 6 cells/mL, respectively. The calibration curve of the corresponding SERS intensity at 1336 cm^{-1} demonstrated a well-maintained linear relationship within 5-10^7 cells/mL of *PA* with a linear correlation coefficient of 0.996. In addition, we compared with other biosensors for the detection of *PA* (Table 1), and the comparison showed that the detection of *PA* using BTMA-SERS microfluidic chip has a larger concentration

Table 1
Performance comparison of BTMA-SERS microfluidic chip with other *PA* biosensors.

Methods	Detection Range	Measured values of LOD	References
Electrochemical	10–10^6 CFU/mL	2 CFU/mL	Zhang et al. (2019)
Fluorescence	10–10^7 CFU/mL	10 CFU/mL	Zhong et al. (2020)
Localized Surface Plasmon Resonance	10–10^3 CFU/mL	10 CFU/mL	Hu et al. (2018)
SERS	7–10^8 CFU/mL	7 CFU/mL	Zhou et al. (2022)
SERS	10–10^7 CFU/mL	10 CFU/mL	Mi et al. (2023)
SERS	5-10^7 cells/mL	5 cells/mL	This work

range and lower detection limit. Additional validate the ability of the chip to be used in clinical samples, we used the chip to measure 12 sputum clinical samples (8 positive patients and 4 healthy laboratory volunteers), the detection results are shown in Fig. S18. Receiver operating characteristic (ROC) curve with an area under the curve (AUC) of 1 indicated the high specificity and accuracy of the chip for determining *PA* clinical samples (Fig. 5g).

Finally, the specificity of BTMA-SERS microfluidic chip was validated by using three other common laboratory bacteria including *E. coli*, *K. pneumoniae*, and *S. aureus* as interferents. 15 μL of immuno-MNPs were added into 1 mL of bacterial solution containing 10^3 cells/mL to incubate and enrich within 15 min. The products were used for SERS detection and 100 μL supernatant was used for blood agar plate coating. As shown in Fig. 5h the capture efficiency of the prepared immuno-MNPs for *PA* was more than 90%, while there was almost no conjugation reaction on the other pathogens. Further, we used the chip to measure samples of each single bacterium and a mixture of four bacteria (*E. coli*, *K. pneumoniae*, *S. aureus* and *PA*) respectively, which were still able to accurately measure the Raman signals of *PA* (10^5 cells/mL). The Raman signals of the three common laboratory bacteria were dynamically variable at negative levels but all were below the LOD of the blank signal, while the Raman signal intensity of *PA* was notably higher than the other three bacterial. Through these experiments, BTMA-SERS microfluidic chip has demonstrated ultra-high resolution and high specificity in bacterial detection.

3.6. Stability performance of BTMA-SERS microfluidic chip

In order to further investigate the potential of BTMA-SERS microfluidic chip for practical applications, we have tested its stability properties. For BTMA-SERS microfluidic chip stability performance test, we kept the position of the chip and its intra-chip MNPs-*PA*-Au@DTNB aggregates fixed and the laser beam was moved ±500 μm laterally with a 100 μm gradient. Based on this, we used SERS-LoC (without BTMA) and BTMA-SERS microfluidic chip (with BTMA) to detect the same concentration of *PA* (10^5cells/mL), respectively. With the results of the 3D data shown in Fig. 6a, it is intuitively clear that the SERS-LoC without BTMA, when the laser beam is moved laterally in the range of

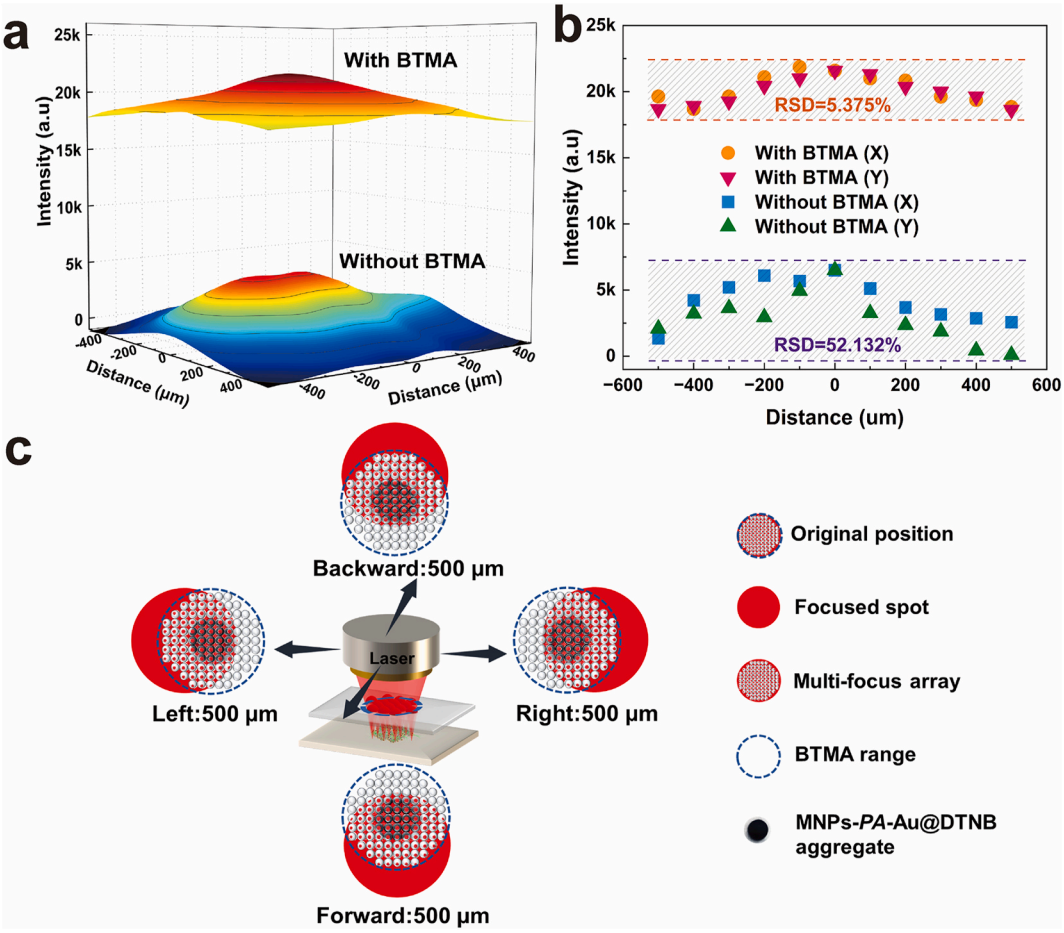

Fig. 6. The results of the double enhancement of signal stability and intensity by using BTMA. (a) The comparison of Raman signal intensity and fluctuation in X–Y plane for the case with and without BTMA, when the excitation beam is laterally moved a distance of ±500 μm. (b) The detailed comparison in the X and Y directions. (c) The MNPs-*PA*-Au@DTNB aggregates can always be covered by the multiple focus arrays formed by the BTMA when the laser beam is moved laterally.

±500 μm, it leads to an uneven distribution of the aggregation hotspots due to the homogeneous sample distribution of the SERS substrate. Meanwhile, the small spot size of the focused beam and the small NA of the objective probe limit its ability to completely cover the sample and its light harvesting efficiency. Finally, as the amount of laser beam displacement increases, the reduction of Raman signal is significant, with RSD of 38.716% and 65.548% in the x and y displacement directions, respectively. The average RSD is 52.132% (Fig. 6b). Under the same conditions, we used BTMA-SERS microfluidic chip to detect the same concentration of *PA,* stability and signal strength are improved. The BTMA acts as micro-lenses to generate the PNJs effect, which converges the incident light and produces a highly focus multi-focal array, increasing the optical power density on the sample surface. The array diameter of the multiple focus arrays is 2 mm, which is larger than the area of the chip detection area, so that when the laser beam is moved laterally, the multiple focus arrays still completely cover the sample in the detection area (Fig. 6c). More importantly, BTMA have a larger NA and a wider range of light collection. The PNJ and DAEs of the BTMA, which enhance the SERS signal by about 4 times, should be particularly noted. At this point, RSD in the X and Y directions are 5.499% and 5.251%, the average RSD is 5.375%, which is about a tenfold improvement in detection stability compared to SERS without the BTMA (Fig. 6b). Therefore, the multiple focus arrays and large NA of the BTMA were utilized to make the focus completely cover the sample on the SERS substrate, which enhanced the light harvesting efficiency and reduced the effect of the lateral movement of the beam on the signal stability. As can be seen, BTMA-SERS microfluidic chip enhanced the detection stability while improving the SERS signal.

4. Conclusion

In this work, a BTMA-SERS microfluidic chip was designed and fabricated that combined a magnet-ultrasound structure, a SERS analysis zone and BTMA for easy integration with both stability and signal enhancement. BTMA are integrated into the chip using vacuum self-assembly hot-pressing method, and the PNJs property of the BTMA is utilized to highly converge the incident light into multiple focus arrays, generates a high-intensity localized surface plasmon resonance, further enhancing the Raman signal. Combined with the large NA and DAEs, which limits the Raman scattering emission angle to ±4.5°, which effectively improves the Raman scattering intensity in the direction of the optical axis and interns efficient far-field energy collection. MNPs and Au@DTNB were used to specifically capture *PA* to form MNPs-*PA*-Au@DTNB, and paired with the coordinated effects of magnetism and ultrasound, flowingly MNPs-*PA*-Au@DTNB was controllably and uniformly focused under the plane of the multiple focus arrays. As a potential clinical pathogen detection tool, we examined PA in whole blood of healthy mice with the LOD and LOQ of 5 cells/mL and 6 cells/mL, respectively. ROC curve with an AUC of 1 indicated the high specificity and accuracy of the chip for determining *PA* clinical samples. More important, BTMA is used as a micro-lens to form a highly focus multiple focus arrays, which can completely cover the samples in the chip, which achieved stable detection of *PA* within ±500 μm of the lateral movement of the laser beam with an RSD of only 5.375%, which reduced the need for precise focusing, while the signal reproducibility had a max RSD of 4.84%. Thus, BTMA-SERS microfluidic chip has both high stability and high sensitivity, which have holds considerable potential for widespread applications in fields like biomedicine, food safety, and other areas requiring the point-of-care testing of pathogenic microorganisms.

CRediT authorship contribution statement

Zhenyong Dong: Writing – review & editing, Writing – original draft, Visualization, Validation, Methodology, Investigation, Formal analysis, Data curation. **Xiaoxian Liu:** Writing – review & editing, Writing – original draft, Visualization, Validation, Methodology, Investigation. **Song Zhou:** Methodology, Investigation, Formal analysis. **Yifan Zhu:** Methodology, Investigation, Formal analysis. **Jin Chen:** Methodology, Investigation. **Yukai Liu:** Investigation. **Xiao Ren:** Investigation. **Yan-qing Lu:** Writing – review & editing, Supervision. **Rui Xiao:** Writing – review & editing, Supervision. **Guanghui Wang:** Writing – review & editing, Supervision, Funding acquisition.

Declaration of competing interest

The authors declare that they have no known competing financial interests or personal relationships that could have appeared to influence the work reported in this paper.

Data availability

Data will be made available on request.

Acknowledgements

This work was supported by the National Natural Science Foundation of China (62375121, 61875083, 61535005), Social Development Project of Jiangsu Province (BE2019761), Natural Science Foundation of Jiangsu Province (BK20211373), the Key Scientific Research Project of Jiangsu Provincial Health Commission (ZD2021060) and the Key Research and Development Program of Shandong Province (2020CXGC011304).

Appendix A. Supplementary data

Supplementary data to this article can be found online at https://doi.org/10.1016/j.bios.2024.116505.

References

Ahi, E.E., Torul, H., Zengin, A., Sucularli, F., Yildirim, E., Selbes, Y., Suludere, Z., Tamer, U., 2022. A capillary driven microfluidic chip for SERS based hCG detection. Biosens. Bioelectron. 195, 113660.

Bai, X., Shen, A., Hu, J., 2020. A sensitive SERS-based sandwich immunoassay platform for simultaneous multiple detection of foodborne pathogens without interference. Anal. Methods 12 (40), 4885–4891.

Du, C.L., Kasim, J., You, Y.M., Shi, D.N., Shen, Z.X., 2011. Enhancement of Raman scattering by individual dielectric microspheres. J. Raman Spectrosc. 42 (2), 145–148.

Fan, M., Andrade, G.F.S., Brolo, A.G., 2020. A review on recent advances in the applications of surface-enhanced Raman scattering in analytical chemistry. Anal. Chim. Acta 1097, 1–29.

Gašparić, V., Taccheo, S., Gebavi, H., Ristić, D., Ivanda, M., 2019. Photonic nanojet mediated Raman enhancement: vertical Raman mapping and simple ray matrix analysis. J. Raman Spectrosc. 51 (1), 165–175.

Geints, Y.E., Zemlyanov, A.A., Minin, O.V., Minin, I.V., 2018. Systematic study and comparison of photonic nanojets produced by dielectric microparticles in 2D- and 3D-spatial configurations. J. Opt. 20 (6).

Hu, J., Fu, K., Bohn, P.W., 2018. Whole-cell Pseudomonas aeruginosa localized surface plasmon resonance aptasensor. Anal. Chem. 90 (3), 2326–2332.

Huang, J.-A., Zhang, Y.-L., Ding, H., Sun, H.-B., 2015. SERS-enabled lab-on-a-chip systems. Adv. Opt. Mater. 3 (5), 618–633.

Kim, S., Ansah, I.B., Park, J.S., Dang, H., Choi, N., Lee, W.-C., Lee, S.H., Jung, H.S., Kim, D.-H., Yoo, S.M., Choo, J., Kim, S.-H., Park, S.-G., 2022. Early and direct detection of bacterial signaling molecules through one-pot Au electrodeposition onto paper-based 3D SERS substrates. Sensor. Actuator. B Chem. 358.

Langer, J., Jimenez de Aberasturi, D., Aizpurua, J., Alvarez-Puebla, R.A., Auguie, B., Baumberg, J.J., Bazan, G.C., Bell, S.E.J., Boisen, A., Brolo, A.G., Choo, J., Cialla-May, D., Deckert, V., Fabris, L., Faulds, K., Garcia de Abajo, F.J., Goodacre, R., Graham, D., Haes, A.J., Haynes, C.L., Huck, C., Itoh, T., Kall, M., Kneipp, J., Kotov, N.A., Kuang, H., Le Ru, E.C., Lee, H.K., Li, J.F., Ling, X.Y., Maier, S.A., Mayerhofer, T., Moskovits, M., Murakoshi, K., Nam, J.M., Nie, S., Ozaki, Y., Pastoriza-Santos, I., Perez-Juste, J., Popp, J., Pucci, A., Reich, S., Ren, B., Schatz, G. C., Shegai, T., Schlucker, S., Tay, L.L., Thomas, K.G., Tian, Z.Q., Van Duyne, R.P., Vo-Dinh, T., Wang, Y., Willets, K.A., Xu, C., Xu, H., Xu, Y., Yamamoto, Y.S., Zhao, B., Liz-Marzan, L.M., 2020. Present and future of surface-enhanced Raman scattering. ACS Nano 14 (1), 28–117.

Li, Y., Hu, Y., Chen, T., Chen, Y., Li, Y., Zhou, H., Yang, D., 2022. Advanced detection and sensing strategies of Pseudomonas aeruginosa and quorum sensing biomarkers: a review. Talanta 240.
Liu, D., Yi, W., Fu, Y., Kong, Q., Xi, G., 2022. In situ surface restraint-induced synthesis of transition-metal nitride ultrathin nanocrystals as ultrasensitive SERS substrate with ultrahigh durability. ACS Nano 16 (8), 13123–13133.
Liu, X.X., Yang, X.S., Li, K., Liu, H.F., Xiao, R., Wang, W.Y., Wang, C.W., Wang, S.Q., 2020. Fe3O4@Au SERS tags-based lateral flow assay for simultaneous detection of serum amyloid A and C-reactive protein in unprocessed blood sample. Sensor Actuat B-Chem 320.
Liu, Z., Han, H., Dai, Y., Li, J., Chen, J., Zhao, J., Xiao, R., 2023. Linear spot Raman detector for the bi-channel immunochromatographic assay to simultaneously detect respiratory viruses. Sensor. Actuator. B Chem. 391.
Ma, L., Ye, S., Wang, X., Zhang, J., 2021. SERS-microfluidic approach for the quantitative detection of miRNA using DNAzyme-mediated reciprocal signal amplification. ACS Sens. 6 (3), 1392–1399.
Mi, F., Guan, M., Wang, Y., Chen, G., Geng, P., Hu, C., 2023. Integration of three non-interfering SERS probes combined with ConA-functionalized magnetic nanoparticles for extraction and detection of multiple foodborne pathogens. Mikrochim. Acta 190 (3), 103.
Mi, Y., Yan, Y., Wang, M., Yang, L., He, J., Jiang, Y., 2022. Cascaded microsphere-coupled surface-enhanced Raman spectroscopy (CMS-SERS) for ultrasensitive trace-detection. Nanophotonics 11 (3), 559–570.
Mungroo, N.A., Oliveira, G., Neethirajan, S., 2015. SERS based point-of-care detection of food-borne pathogens. Microchim. Acta 183 (2), 697–707.
Pahl, T., Hüser, L., Hagemeier, S., Lehmann, P., 2022. FEM-based modeling of microsphere-enhanced interferometry. Light: Adv. Manuf. 3 (4).
Panneerselvam, R., Sadat, H., Hohn, E.M., Das, A., Noothalapati, H., Belder, D., 2022. Microfluidics and surface-enhanced Raman spectroscopy, a win-win combination? Lab Chip 22 (4), 665–682.
Ruzankina, I., Mukhin, N., Mermoul, A., Parfenov, V., Fron, E., Ferrini, G., 2022. Surface optical sensitivity enhanced by a single dielectric microsphere. Opt Express 30 (24), 43021–43036.
Song, D., Yang, R., Fang, S., Liu, Y., Long, F., Zhu, A., 2018. SERS based aptasensor for ochratoxin A by combining Fe(3)O(4)@Au magnetic nanoparticles and Au-DTNB@Ag nanoprobes with multiple signal enhancement. Mikrochim. Acta 185 (10), 491.
Spaziani, S., Quero, G., Manago, S., Zito, G., Terracciano, D., Macchia, P.E., Galeotti, F., Pisco, M., De Luca, A.C., Cusano, A., 2023. SERS assisted sandwich immunoassay platforms for ultrasensitive and selective detection of human Thyroglobulin. Biosens. Bioelectron. 233, 115322.
Wang, J., Wu, X., Wang, C., Shao, N., Dong, P., Xiao, R., Wang, S., 2015. Magnetically assisted surface-enhanced Raman spectroscopy for the detection of Staphylococcus aureus based on aptamer recognition. ACS Appl. Mater. Interfaces 7 (37), 20919–20929.
Wang, M., Yan, Y., Mi, Y., Jiang, Y., 2022. Flexible microsphere-coupled surface-enhanced Raman spectroscopy (McSERS) by dielectric microsphere cavity array with random plasmonic nanoparticles. J. Raman Spectrosc. 53 (7), 1238–1248.
Wang, Y., Li, Q., Shi, H., Tang, K., Qiao, L., Yu, G., Ding, C., Yu, S., 2020. Microfluidic Raman biochip detection of exosomes: a promising tool for prostate cancer diagnosis. Lab Chip 20 (24), 4632–4637.
Wu, L., Liu, X., Zhang, Y., Yang, Z., Chen, L., Zong, S., Li, J., Cui, Y., Wang, Z., 2024. A hand-powered SERS-microfluidic chip for circulating tumor DNA detection from whole blood. Sensor. Actuator. B Chem. 401.
Xie, M., Zhu, Y., Li, Z., Yan, Y., Liu, Y., Wu, W., Zhang, T., Li, Z., Wang, H., 2024. Key steps for improving bacterial SERS signals in complex samples: separation, recognition, detection, and analysis. Talanta 268 (Pt 1), 125281.
Xie, T., Xu, D., Shang, Y., Li, Y., Gu, Y., Yang, G., Qu, L., 2023. Highly sensitive SERS detection of IL-6 in serum by Au@Fe3O4 nanoring-based sandwich immunoassay. Sensor. Actuator. B Chem. 375.
Xiong, Q., Lim, C.Y., Ren, J., Zhou, J., Pu, K., Chan-Park, M.B., Mao, H., Lam, Y.C., Duan, H., 2018. Magnetic nanochain integrated microfluidic biochips. Nat. Commun. 9 (1), 1743.
Yan, Y., Xing, C., Jia, Y., Zeng, Y., Zhao, Y., Jiang, Y., 2015. Self-assembled dielectric microsphere array enhanced Raman scattering for large-area and ultra-long working distance confocal detection. Opt Express 23 (20), 25854–25865.
Yang, H., Trouillon, R., Huszka, G., Gijs, M.A., 2016. Super-resolution imaging of a dielectric microsphere is governed by the waist of its photonic nanojet. Nano Lett. 16 (8), 4862–4870.
Yang, K., Zhang, C., Zhu, K., Qian, Z., Yang, Z., Wu, L., Zong, S., Cui, Y., Wang, Z., 2022. A programmable plasmonic gas microsystem for detecting arbitrarily combinated volatile organic compounds (VOCs) with ultrahigh resolution. ACS Nano 16 (11), 19335–19345.
Yousefi, M., Scharf, T., Rossi, M., 2021. Photonic nanojet generation under converging and diverging beams. J. Opt. Soc. Am. B 38 (2).
Yu, Q., Wu, T., Tian, B., Li, J., Liu, Y., Wu, Z., Jin, X., Wang, C., Wang, C., Gu, B., 2024. Recent advances in SERS-based immunochromatographic assay for pathogenic microorganism diagnosis: a review. Anal. Chim. Acta 1286, 341931.
Zhang, P., Chen, X., Yang, H., 2020. Large-scale fabrication of photonic nanojet array via template-assisted self-assembly. Micromachines 11 (5).
Zhang, P., Yan, B., Gu, G., Yu, Z., Chen, X., Wang, Z., Yang, H., 2022. Localized photonic nanojet based sensing platform for highly efficient signal amplification and quantitative biosensing. Sensor. Actuator. B Chem. 357.
Zhang, X., Xie, G., Gou, D., Luo, P., Yao, Y., Chen, H., 2019. A novel enzyme-free electrochemical biosensor for rapid detection of Pseudomonas aeruginosa based on high catalytic Cu-ZrMOF and conductive Super P. Biosens. Bioelectron. 142, 111486.
Zhong, Z., Gao, R., Chen, Q., Jia, L., 2020. Dual-aptamers labeled polydopamine-polyethyleneimine copolymer dots assisted engineering a fluorescence biosensor for sensitive detection of Pseudomonas aeruginosa in food samples. Spectrochim. Acta Mol. Biomol. Spectrosc. 224, 117417.
Zhou, S., Guo, X., Huang, H., Huang, X., Zhou, X., Zhang, Z., Sun, G., Cai, H., Zhou, H., Sun, P., 2022. Triple-function Au-Ag-stuffed nanopancakes for SERS detection, discrimination, and inactivation of multiple bacteria. Anal. Chem. 94 (15), 5785–5796.